Computers and Concrete, Vol. 7, No. 2 (2010) 87-102
DOI: http://dx.doi.org/10.12989/cac.2010.7.2.087

The virtual penetration laboratory: new developments for projectile penetration in concrete

Mark D. Adley*, Andreas O. Frank, Kent T. Danielson,
Stephen A. Akers and James L. O'Daniel

U.S. Army Engineer Research and Development Center, Geotechnical and Structures Laboratory, 3909 Halls Ferry Road, Vicksburg, MS 39180-6199, USA

(Received July 1, 2009, Accepted July 21, 2009)

Abstract. This paper discusses new capabilities developed for the Virtual Penetration Laboratory (VPL) software package to address the challenges of determining Penetration Resistance (PR) equations for concrete materials. Specifically, the paper introduces a three-invariant concrete constitutive model recently developed by the authors. The Advanced Fundamental Concrete (AFC) model was developed to provide a fast-running predictive model to simulate the behavior of concrete and other high-strength geologic materials. The Continuous Evolutionary Algorithms (CEA) automatic fitting algorithms used to fit the new model are discussed, and then examples are presented to demonstrate the effectiveness of the new AFC model. Finally, the AFC model in conjunction with the VPL software package is used to develop a PR equation for a concrete material.

Keywords: penetration mechanics; constitutive modeling; evolutionary algorithms.

1. Introduction

The Geotechnical and Structures Laboratory of the U.S. Army Engineer Research and Development Center (ERDC) has conducted a significant amount of projectile penetration research. These efforts have included numerous projectile penetration experiments using the ERDC 83-mm ballistic research facility (Frew *et al.* 1993), extensive material property experiments that characterize target mechanical behavior and provide data for fitting constitutive models (Akers *et al.* 1995), and numerous fully-first-principle calculations of various penetration events (Adley *et al.* 1996). Our research is focused around gathering data and gaining insight into the processes of penetration mechanics. One of the primary goals of our research is to develop more accurate and robust material models that can be more easily used by an analyst. As the complexity of constitutive models increases, it also becomes increasingly difficult to fit the laboratory material property data to these models. Therefore, a second focus of our efforts is to develop methodologies to reduce the time and effort required to fit the material models.

As mentioned previously, projectile penetration events can be simulated by using fully "first-principle" methods such as "hydrocodes". This is accomplished by discretizing both the projectile and the target into a finite number of pieces and allowing the first-principle physics, i.e., conservation of mass, momentum, and energy, to dictate the penetration event. Over the past few decades, many hydrocode techniques have been developed. Typically, these codes differ in how they discretize the

* Corresponding author, Ph.D., E-mail: mark.d.adley@usace.army.mil

computational domain by using either an Eulerian, Lagrangian, or "mixed" formulation. The mixed formulation might be an Arbitrary Lagrange Euler (ALE) formulation or a coupled formulation that links a Lagrangian code with an Eulerian code. However, these computational methods are all extremely resource intensive. Therefore, a third focus of our research efforts is the development of numerical methods for simulating projectile penetration that replace the finite element model of the target with penetration resistance equations that represent the resistance of a target material to penetration.

In this paper, we discuss the development of a three-invariant constitutive model for simulating concrete penetration by projectiles. We focused our efforts on the EPIC Lagrangian hydrocode (Johnson *et al.* 2001), because the source code is readily available to us, and we have used this code for a number of years. It was our intention to develop a relatively simple yet robust model that includes a three-invariant failure surface because such a model is not currently available in the production version of EPIC. For example, two-invariant models such as the HJC (Holmquist *et al.* 1993) and Hull (Johnson *et al.* 2001) concrete models have their failure surface completely described by only the first two invariants of the stress tensor. It has been shown that the failure surface for many geomaterials (including concrete) may be dependent on all three stress invariants (Fossum and Brannon 2006). For example, the strength observed during compression at a given level of pressure is typically greater than the extension strength at the same pressure. This is illustrated in Fig. 1, which shows a hypothetical failure surface for concrete in the principal stress space, i.e., meridonial and octahedral planes (Fossum and Brannon 2006).

In this paper, we also discuss the automatic fitting (i.e., through a numerical algorithm) of our constitutive model to various laboratory material property data. Since the VPL code contains several complex material models such as the microplane model (Bažant *et al.* 1996, 2000) it has become increasingly difficult to fit laboratory material property data to the VPL models. However, since the use of these sophisticated models has become more widespread (e.g., Ožbolt *et al.* 2005, 2008) it has become increasingly important to be able to readily fit these types of complex models. Therefore, we developed a material model fitting program to accomplish that goal. We will demonstrate the use of this automatic fitting program.

Finally, we will present validation examples that use the AFC model and the material fits generated to simulate projectile penetration experiments. We will also use the validated model and the associated fits in the VPL software package to generate a PR equation that will be used to simulate the aforementioned penetration experiments.

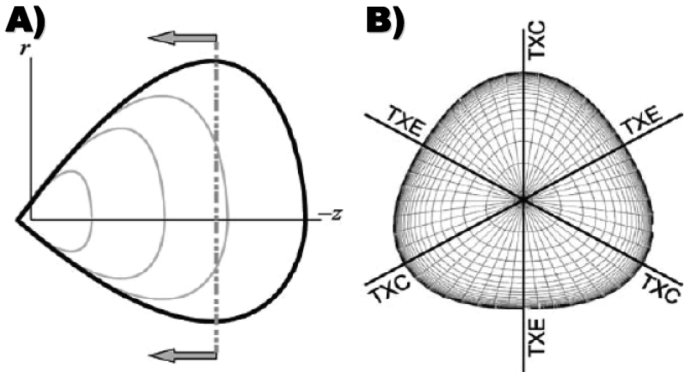

Fig. 1 A hypothetical failure surface for concrete shown in principal stress space, as follows: A) the meridional view and B) the octahedral view. Adapted from Fossum *et al.* (2006)

2. Constitutive model development

2.1. Model description

Our constitutive model is a three-invariant plasticity model. The model simulates irreversible hydrostatic crushing, material yielding, plastic flow, and damage. The model has a non-linear pressure-volume relationship and a linear shear relationship (i.e., constant G). The model also includes strain-rate effects for the failure surface (i.e., increasing shear strength with increasing strain rates). As with most of the simple constitutive models for concrete, our model separates the hydrostatic response from the deviatoric response. Thus, the hydrostatic and deviatoric responses are independently calculated without providing any coupling between the two (i.e., no volumetric strain due to pure deviatoric loading can develop).

First, we will describe the hydrostatic behavior of our model, which includes a non-linear bulk modulus and irreversible volumetric crushing that contributes to material damage. More specifically, the compressive hydrostatic behavior can be separated into three distinct regions described by an initial elastic zone, followed by an irreversible crushing response, and finally an elastic locking region. Furthermore, the model treats initial loading, unloading, and reloading differently.

The initial elastic zone for the model only occurs for volume strains below the crushing volume strain value (U_{crush}). Initial loading, unloading, and reloading in the elastic zone all follow linear elastic behavior defined by the elastic bulk modulus ($K_e=P_{crush}/U_{crush}$), where P_{crush} is the maximum attainable pressure for the initial elastic zone.

The irreversible crushing response occurs for all materials in which the volume strain exceeds the crushing volume strain value (U_{crush}) but has not exceeded the locking volume strain value (U_{lock}). The crushing region is defined by letting the origin of the crushing response coincide with the point in pressure-volume space (P_{crush}, μ_{crush}). Hence, that same point also coincides with the ending of the initial elastic zone. The crushing region is characterized by permanent volume compaction and follows the following third-order polynomial equation.

$$P = K_1\mu + K_2\mu^2 + K_3\mu^3 \tag{1}$$

where K_1, K_2, K_3 are input parameters, P is the mean normal stress (pressure), and μ is a measure of volumetric strain. It should be noted that this equation uses the soil mechanics sign convention (compression > 0), which means that the pressure (P) as computed by the previous equation is equal to the first invariant of the stress tensor (I_1) multiplied by -1, i.e., $I_1=-P$. In the crushing region, unloading and reloading are non-linear with the bulk modulus varying linearly between K_e and K_{lock} as μ varies between U_{crush} and U_{lock}. However, since the change in μ during a typical unload-reload cycle in the crush zone is generally only a small percentage of the value of (U_{lock} - U_{crush}), the response in most cases is nearly linear.

The linear elastic locking region in the model is defined by a locking bulk modulus (K_{lock}) and occurs for volume strains above the locking value for volumetric strain (U_{lock}). Unloading and reloading in the locking region are purely linear elastic and also follow the locking bulk modulus (K_{lock}).

The tensile hydrostatic behavior of the model is always defined by linear elastic behavior and follows a bulk modulus that is between the elastic bulk modulus (K_e) and the locking bulk modulus (K_{lock}), depending on the level of permanent volumetric crushing. For example, the tensile hydrostatic behavior follows the elastic bulk modulus (K_e) for any material in which volume strains have not exceeded the initial crushing volume strain value (U_{crush}). However, if the material has

exceeded U_{crush}, the tensile hydrostatic behavior follows an elastic bulk modulus that is greater than or equal to K_e and less than or equal to K_{lock}. Since the change in μ during a typical unload-reload cycle in the tensile zone is generally only a small percentage of the value of (U_{lock} - U_{crush}), the response in most cases is nearly linear.

Next, we will describe the shear behavior of the model, which includes material yielding plastic flow and damage. Notice that an engineering mechanics sign convention has been used, hence the mean normal stress (pressure) values less than zero denote compression. The compression yield surface is represented by the following two equations, depending on whether the hydrostatic component of the stress state is in compression or tension.

For stress states where the first invariant of the stress tensor (I_1) is less than or equal to zero (indicative of compression), the failure surface is expressed as

$$S_Y = (C_1 - (C_2 + (C_1 - C_2)D)e^{A_n I_1} - C_4 I_1)(1 + C_3 Ln(\dot{\varepsilon}_n)) \tag{2}$$

where C_1, C_2, C_3, C_4, and A_n are constants that are greater than or equal to zero, D is a damage parameter that varies between 0 and 1, and $\dot{\varepsilon}_n$ is an effective deviatoric strain rate that is normalized to a reference rate that is provided as input. It should also be noted that the values of C_1 and C_2 must satisfy the constraint $C_1 \geq C_2$.

For stress states where the first invariant of the stress tensor (I_1) is greater than zero (indicative of tension), the failure surface is expressed as

$$S_Y = (C_1 - (C_2 + (C_1 - C_2)D))(1 + C_3 Ln(\dot{\varepsilon}_n))(T_{\max} - I_1)/T_{\max} \tag{3}$$

where T_{max} is the maximum allowable tensile pressure, and the value of S_y is restricted to values that are greater than or equal to zero.

The third-invariant dependence of the failure surface is computed using the Lode angle (Chen and Han 1988). For example, a discrete extension failure surface value is computed by first computing the value of the compression failure surface at the stress state of interest, and then multiplying the compression failure surface value by a factor that is a function of the third invariant of the deviatoric stress tensor. Specifically, the Lode angle is computed, and then the value of the aforementioned factor is computed by evaluating either the William-Warnke Lode function or the Gudehus Lode function (Fossum and Brannon 2006).

As stated previously, our constitutive model also accounts for material damage that develops during the course of stress/strain loading histories. This material damage effectively provides a reduced failure surface due to excessive plastic shear strain as well as excessive hydrostatic crushing. The value of material damage is quantified using a scalar damage parameter (D) that is computed by evaluating the following damage equation.

$$D = \sum\left(\frac{\Delta\varepsilon_p}{-I_1 D_1} + \frac{\Delta\mu_p}{1.5 U_{lock}}\right) \tag{4}$$

where D_1 is an input parameter that is greater than zero, values of the expression ($-I_1 D_1$) are restricted to values greater than 0.01, $\Delta\varepsilon_p$ is an increment in the effective deviatoric plastic strain, $\Delta\mu_p$ is an increment of volumetric plastic strain, and U_{lock} is the locking volumetric strain value previously described. Notice that the material damage parameter (D) is included in calculation of the failure surface as shown above in Eq. (2) and Eq. (3).

2.2. Model fitting

The automatic fitting program used to fit the AFC model is described in this section. Although genetic algorithms have been successfully used in a wide range of engineering optimization problems (e.g., Parichatprecha and Nimityongskul 2009), the developers of the VPL code have opted to use Continuous Evolutionary Algorithms (Furukawa, Sugata, Yoshimura, and Hoffman 2002) (CEA) in conjunction with the Levenberg-Marquardt Algorithm (Marquardt 1963) (LMA) to evaluate the parameter values used in the material model of interest. These algorithms are used to minimize the weighted sum of the squared residuals merit function given by

$$\Phi(\bar{a}) = \sum_{i=1}^{n} w_i [\sigma_i - \hat{\sigma}_i(\varepsilon, \bar{a})]^2 \tag{5}$$

where σ represents the stress values measured in material property experiments, $\hat{\sigma}$ represent the stress values predicted by the material model, which are a function of the strain (ε) and the vector of material model parameter values ($\bar{a}$), and w is a weighting factor.

In CEA, a trial solution is a vector representation of the parameter set ($\bar{a}$). The algorithm employed in this work selects a number (m) of initial trial solutions where the parameter values in each of the m vectors are selected at random. The following operations are then completed in a loop that is only terminated when a convergence criterion is satisfied, i.e., the merit function has reached an acceptably small value.

The operations performed each time through the loop (in each generation), in the order of calculation, are: (1) evaluate the merit function (Φ) for each of the m trial solutions (individuals), (2) identify and save the solution that provided the smallest value of the merit function for use in the next generation (the most fit individual), (3) use the method of steepest descent, starting at the best solution (the elite individual identified in the previous operation) to determine a new trial solution that will replace the worst solution (least fit individual), and (4) recombine the current trial solutions to obtain the additional (m-1) trial solutions required, where the probability of a vector's participation in the recombination (mating) process depends on its' merit function value (fitness). It is clearly seen by the vocabulary used in the description of CEA algorithms that they are inspired by biological evolution processes.

The recombination (mating) algorithm used in the current work is represented by the following equations.

$$\begin{aligned} \bar{a}_i^* &= (1-\alpha)\bar{a}_i + \alpha\bar{a}_j \\ \bar{a}_j^* &= \alpha\bar{a}_i + (1-\alpha)\bar{a}_j \end{aligned} \tag{6}$$

where α is a scalar value that is defined by a normal distribution with a mean of 0 and a specified standard deviation, and the parents ($\bar{a}_i$ and $\bar{a}_j$) are selected at random from the mating pool. Since the probability of a solution (individual) being selected to participate in the mating process depends on the value of its merit function (level of fitness), this search algorithm moves toward a solution that minimizes the merit function and provides a best fit to the material property data used in the merit function.

2.3. Model response

We fit our constitutive material model using the available laboratory material property data for two different conventional strength concrete materials, which we shall call materials WES5000 and

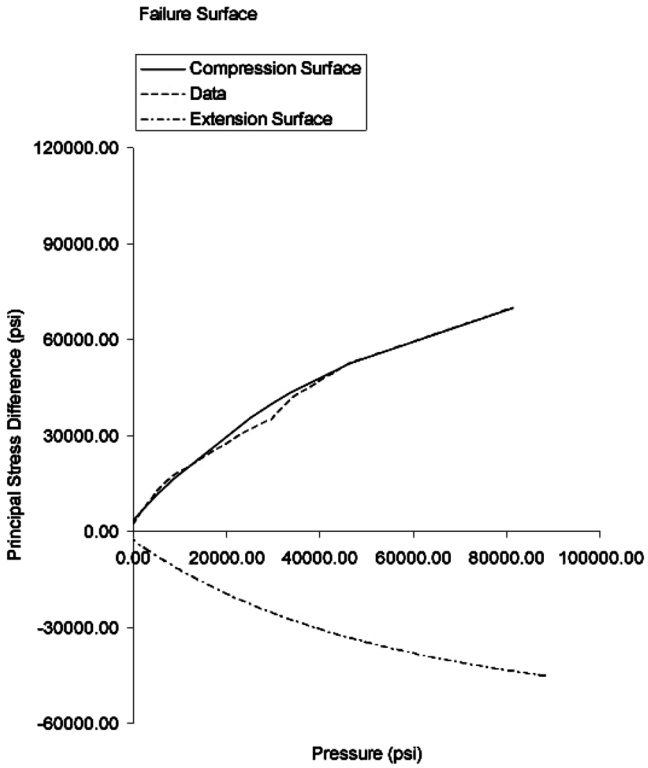

Fig. 2 AFC failure surface fit to WES5000 concrete data

CSPC. These fits were generated using the automatic fitting program described above in conjunction with a finite element driver program that can simulate the appropriate loading and strain conditions (i.e., boundary conditions) from results of the laboratory material property testing. Specifically, we used quasi-static hydrostatic compression, unconfined compression, uniaxial strain compression, triaxial compression, and direct-pull laboratory material property data to generate our material model constants. It should be noted that we did not have any rate dependent data and thus could not fit the failure surface rate parameter using the automatic fitting code. Instead, this parameter was fit using numerical simulations in conjunction with the projectile penetration experiments described below.

The automatically generated fit to concrete material WES5000 is shown in Figs 2-4. These figures employ the soil mechanics sign convention where compression is positive. As shown in Fig. 2, the model is able to differentiate between the extension and compression failure surfaces due to the inclusion of the third invariant. The failure surface data is used by the automatic fitting code to determine the material model parameters that define the shape of the failure surface. The parameters that define the pressure-volume behavior of the model were determined by automatically fitting the uniaxial strain data shown in Fig. 3. The fitting code determined the damage parameter by matching the softening behavior observed in various triaxial compression tests, e.g. Fig. 4.

The automatically generated fit to concrete material CSPC is shown in Figs 5-7. These figures also employ the soil mechanics sign convention where compression is positive. As shown in Fig. 5, the model is able to differentiate between the extension and compression failure surfaces due to the inclusion of the third invariant. The failure surface data is used by the automatic fitting code to

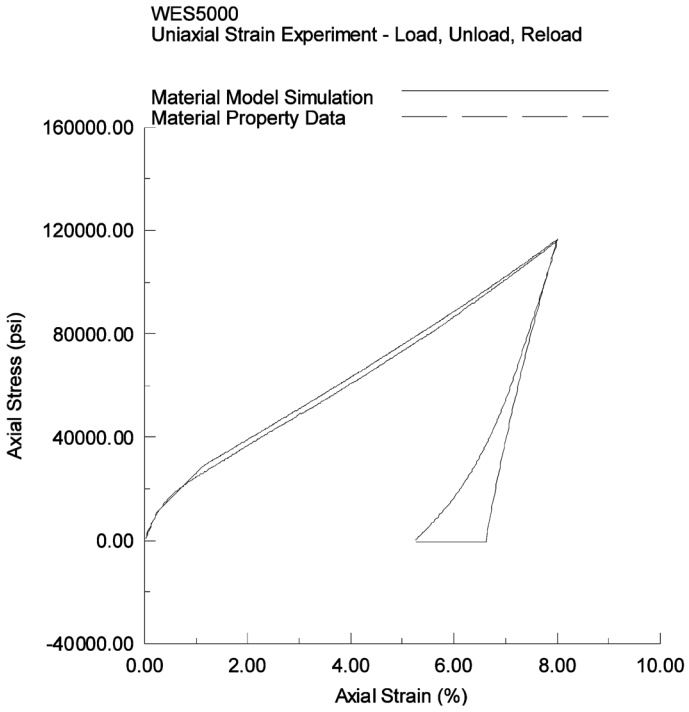

Fig. 3 AFC model fit to WES5000 uniaxial strain test data

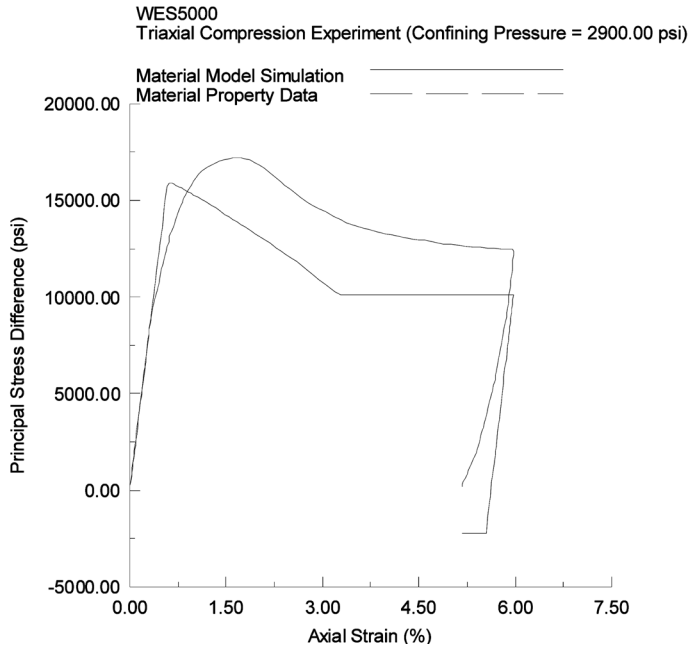

Fig. 4 AFC model fit to WES5000 triaxial compression data

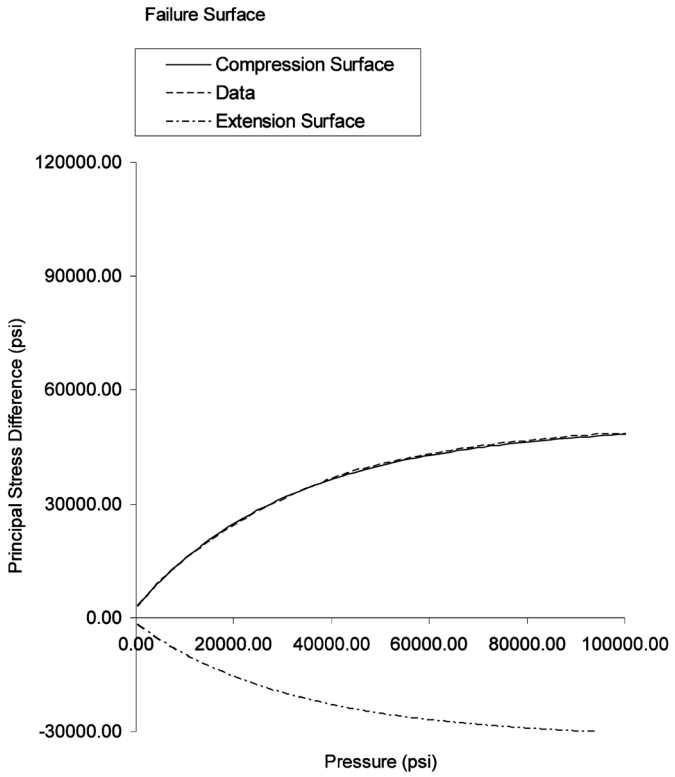

Fig. 5 AFC failure surface fit to CSPC concrete data

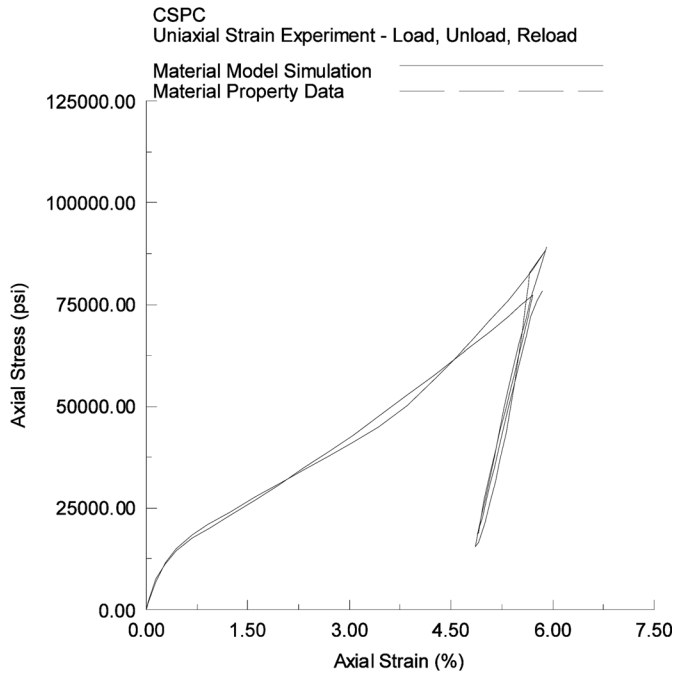

Fig. 6 AFC model fit to CSPC uniaxial strain test data

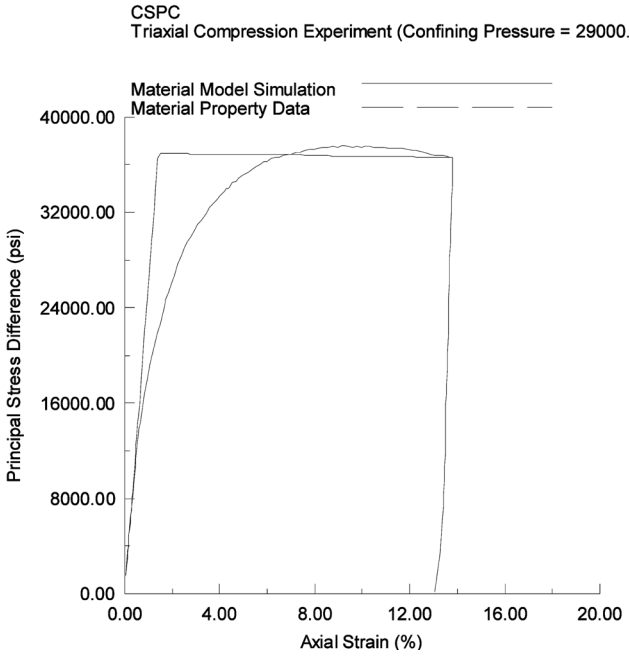

Fig. 7 AFC model fit to CSPC triaxial compression data

determine the material model parameters that define the shape of the failure surface. The parameters that define the pressure-volume behavior of the model were determined by automatically fitting the uniaxial strain data shown in Fig. 6. Finally, the fitting code determined the damage parameter by matching the softening behavior observed in various triaxial compression tests, e.g., Fig. 7.

2.4. Model implementation and testing

We implemented the constitutive material model described above into the EPIC hydrocode. The implementation was relatively straight forward, and we will not discuss this in any more detail. In order to test the response of this material model, we performed numerical simulations of various penetration experiments conducted at ERDC. These simulations included both projectile perforation as well as deep penetration. We discuss the results from these simulations along with corresponding comparisons to the experimental data below.

3. Perforation simulations

3.1. Perforation experiments

We based our calculations on a series of perforation experiments conducted at ERDC (Cargile 1999). The experiments were conducted with a 2.3-kg ogival nose projectile (CRH=3.0, L/D=7.0, and D=50.8 mm) launched into three unreinforced concrete slabs with thicknesses of 127, 216, and 254 mm. Each of the slabs was constructed in a steel culvert with a nominal diameter of 1.52 m, providing a near infinite width for these perforation events (i.e., a target width to projectile diameter ratio of 30). All the

experiments were conducted under "near" normal impact conditions, i.e., angle-of-obliquity and angle-of-attack were less than 1 degree, with an impact velocity of approximately 310 m/sec. The slabs were constructed from the WES5000 concrete material. The experiments were designed to challenge the numerical simulations by providing three distinctly different target responses (i.e., a relatively thin slab providing little resistance, a typical slab providing nominal resistance, and finally a relatively thick slab approaching the perforation limit thickness of the projectile). Thereby, these experiments provide a good baseline for comparison with the impact and exit phase of projectile penetration (Cargile 1999), which is typically characterized by low confinement stress states under compression, extension, and/or tension for the target material. All the experiments resulted in complete perforation of the concrete slabs. Fig. 8 shows representative results from these perforation experiments. Shown are typical projectile exit velocities and the posttest concrete damage in terms of the final impact and exit crater profiles.

3.2. 2D Perforation simulations

We conducted 2D axi-symmetric EPIC simulations of the perforation experiments discussed above and illustrated in Fig. 8. Our finite element models were developed to focus on the target responses. Therefore, we used a fairly low fidelity input for the projectile (617 elements) and a high fidelity input for each of the target slabs, i.e., 4919, 8379, and 10001 elements for the 127-, 216-, and 254-mm slabs, respectively. It should be noted that our finite element models use linear triangular elements. We used the experimentally determined projectile exit velocities and the final crater profiles from Fig. 8 as the metrics to evaluate our simulations.

Fig. 9 shows a snapshot at 10 msec from the 127-mm-slab EPIC simulations. The crater shape observed in the relevant experiment is superimposed on the target shown in Fig. 9. The predicted exit velocity is in very close agreement to the value recorded in the experiment (see Fig. 8), and the crater shape is reasonable.

Fig. 10 shows a snapshot at 10 msec from the 216-mm-slab EPIC simulations. The crater shape observed in the relevant experiment is superimposed on the target shown in Fig. 10. The predicted exit velocity is in good agreement with the value recorded in the experiment (see Fig. 8), and the

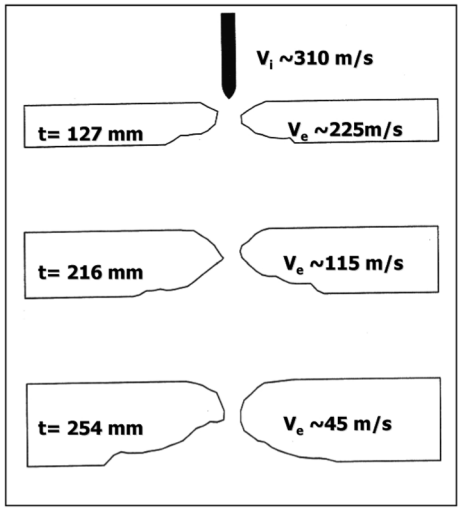

Fig. 8 Representative results from various perforation experiment (Cargile 1999). Shown are the impact (V_i) and exit (V_e) velocities as well as the final crater shapes

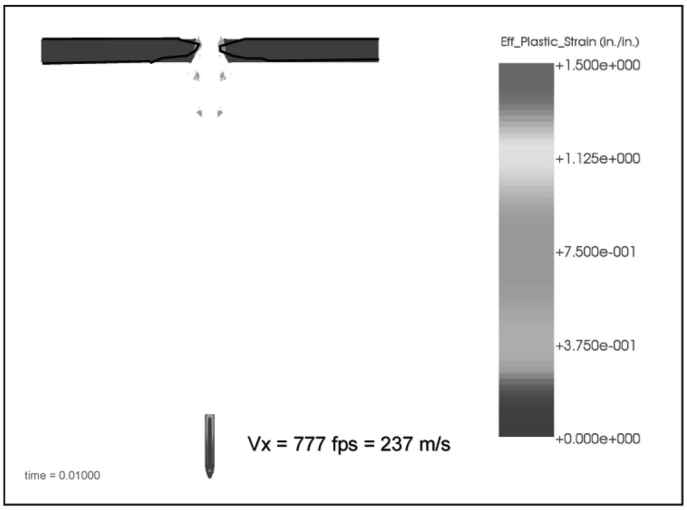

Fig. 9 EPIC penetration simulation using the AFC model-127-mm-thick concrete target

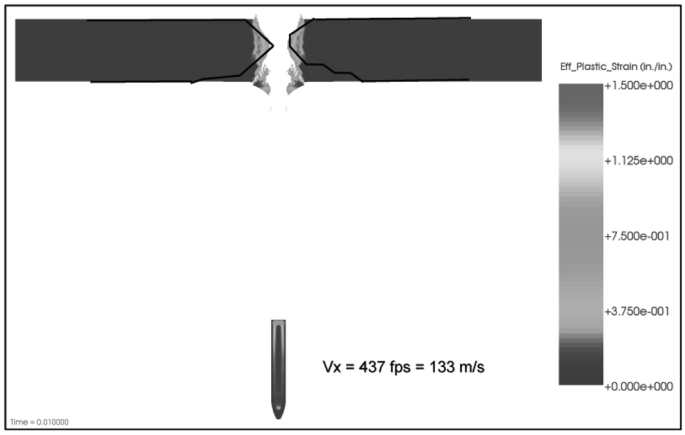

Fig. 10 EPIC penetration simulation using the AFC model-216-mm-thick concrete target

crater shape is also in close agreement with the experimental data.

Fig. 11 shows a snapshot at 15 msec from the 254-mm slab EPIC simulations. The crater shape observed in the relevant experiment is superimposed on the target shown in Fig. 11. Since the target used in this example is close to the perforation limit thickness, this is a very challenging problem. However, in spite of that fact, the predicted exit velocity is reasonable, and the impact crater shape is in excellent agreement with the data. The predicted shape of the exit crater is reasonable, but it is much smaller than the exit crater observed in the experiment.

4. Penetration simulations

4.1. Penetration experiments

We based these calculations on a series of penetration experiments also conducted at ERDC

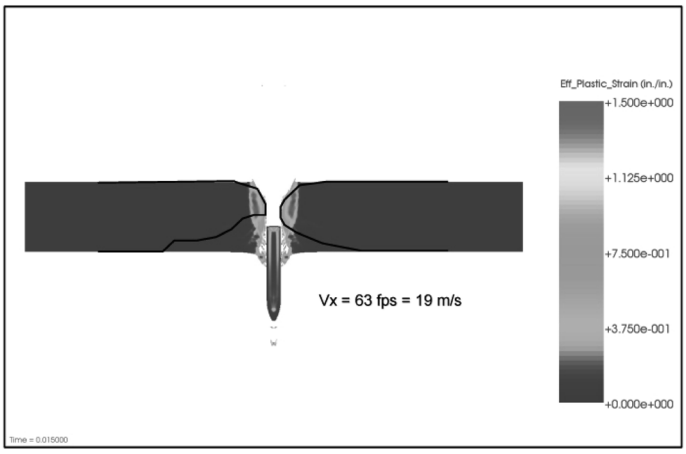

Fig. 11 EPIC penetration simulation using the AFC model-254-mm-thick concrete target

(Cargile 1999). The experiments were conducted with a 0.9-kg ogival nose projectile (CRH=2.0, L/D=9.0, and D=26.9 mm) launched into a 1.22-m-diameter target with a depth of 1.83 m. These targets were designed to be nearly a half space providing a relatively large depth and width (i.e., the target width to diameter ratio was 45, and the target depth to projectile diameter ratio was 68). The targets were unreinforced and constructed in a steel culvert with the CSPC concrete material. All the experiments were conducted under "near" normal impact conditions, i.e., angle-of-obliquity and angle-of-attack were less than 1 degree. The impact velocities were varied from 277 to 800 m/sec. The experiments were designed to allow for near rigid-body penetration events (i.e., a robust thick-walled projectile). The data recorded from these experiments was the depth of penetration versus impact velocity. None of the experiments resulted in the projectile penetrating more than half the target depth. Thereby, these experiments provide a good baseline for comparison with the tunneling phase of projectile penetration (Cargile 1999), which is typically characterized by high confinement stress states under compression for the target material.

4.2. 2D Penetration simulations

We conducted 2D axi-symmetric EPIC simulations of the penetration experiments discussed above. Our finite element models were developed to focus on the target responses, and therefore, we used a fairly low fidelity for the projectile (264 elements) and a higher fidelity for the target slab (14960 elements). It should be noted that our finite element models use linear triangular elements. We used the experimentally determined projectile penetration depth as the metric to evaluate our simulations.

Fig. 12(a) shows a snapshot at 1.2 msec from the 300-m/sec EPIC simulation, and Fig. 12(b) shows a snapshot at 2 msec from the 800-m/sec EPIC simulation. As shown in Fig. 12, these are deep penetration simulations where the projectile spends the majority of the event in a tunneling mode.

Fig. 13 is a comparison of the penetration depth versus velocity for the EPIC simulations and the experimental data. The depth of penetration predictions are in close agreement with the experiments for the two lower velocity simulations. However, when the impact velocity approaches 800 m/s, the fidelity of the predictions appears to decrease.

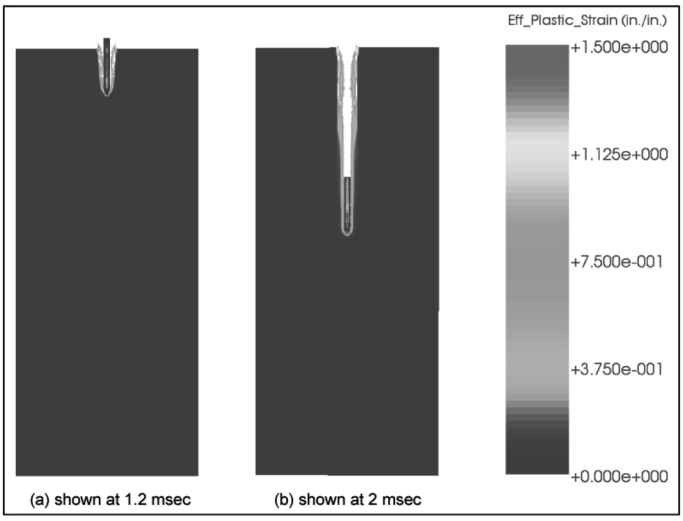

Fig. 12 EPIC penetration simulations using the AFC model for impact velocities of (a) 300 m/s, and (b) 800 m/s

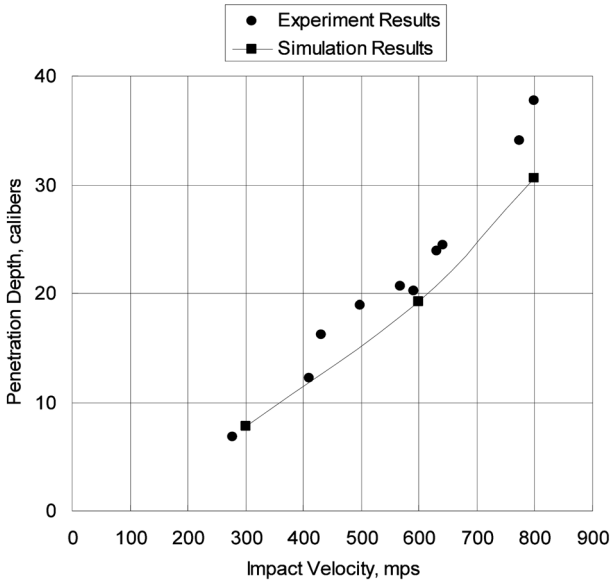

Fig. 13 EPIC penetration simulation results using the AFC model versus experimental data from ballistic experiments (Cargile 1999)

5. CSPC penetration resistance equation

The VPL software package includes a one-dimensional finite element code that is used to solve cavity expansion simulations, and a rigid-body trajectory code that uses PR equations to model the target material. The process used to develop PR equations is briefly discussed below. A more comprehensive discussion of this topic is available in the paper by Adley *et al.* (2007).

The methodology employed in VPL to develop PR equations involves using the finite element

method to solve the equations governing the dynamic expansion of a spherical cavity in a target material. The first step in the process involves the solution of a series of cavity expansion problems where each problem is defined as the opening of a spherical cavity at a constant expansion velocity. Each cavity expansion solution is run until the radial (normal to cavity wall) stress approaches a constant value. Each of those solutions represents a point in radial stress versus radial velocity space.

The second step in the process involves the determination of the quadratic equation that best fits the aforementioned data points in a least squares sense. This equation represents the resistance of the target to the opening of a cavity as a function of the cavity expansion velocity.

The third step requires the transformation of the cavity expansion resistance equation to a penetration resistance equation. This is accomplished by replacing the radial cavity expansion velocity with the component of the projectile's velocity that is normal to the surface of the projectile at the point under consideration, e.g., the center of an element face that is located in the outer surface of the finite element mesh of the projectile. The resisting stress predicted by the transformed equation is then interpreted as the normal stress that is acting on the surface of the projectile at the point under consideration, i.e., the penetration resistance of the target.

The completion of the aforementioned three tasks results in the development of the penetration resistance equation. The equation can then be implemented in a rigid-body trajectory code to study the loading history predicted by the penetration resistance equation and the fidelity of the penetration trajectory predictions. Assuming the results of that validation process produce encouraging results, the equation can then be implemented in a finite element code to study the structural response of projectiles subjected to impact and penetration events.

The AFC concrete model and the fit for CSPC concrete discussed previously is used in conjunction with the cavity expansion code to develop a PR equation for CSPC concrete. The PR equation is shown in Fig. 14 along with the numerical data points that represent the cavity expansion solutions. The PR equation shown in Fig. 14 is used in the VPL trajectory code to

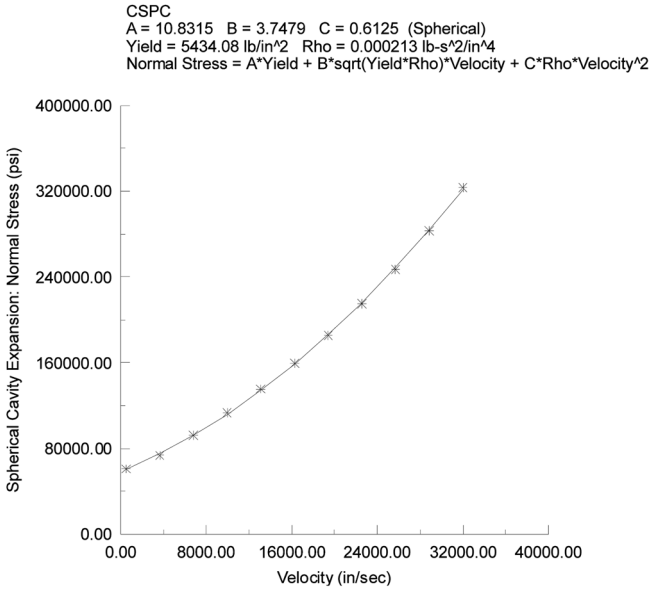

Fig. 14 The CSPC PR equation developed in the VPL code

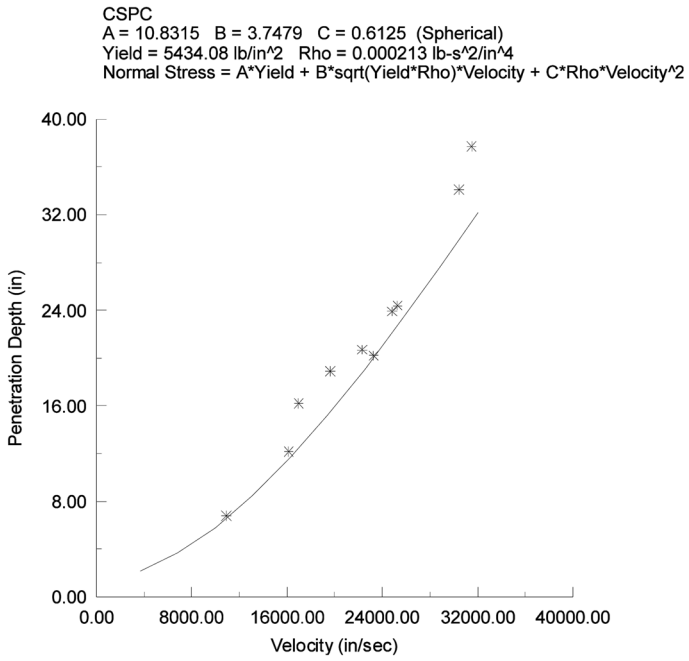

Fig. 15 Trajectory code predictions (solid line) conducted using the CSPC PR equation and compared to experimental data (Cargile 1999)

simulate the deep penetration experiments discussed in the previous section, i.e., the PR equation is used to model the target. A comparison between the VPL predictions and the experimental data is shown in Fig. 15. As shown in Fig. 15, the fidelity of the predictions rivals the fidelity of the full finite element simulations presented in the previous section, even though the VPL simulations require only a small fraction of the computer time.

6. Conclusions

This paper presented a new three-invariant constitutive model for concrete called the AFC model. The automatic fitting algorithms used to determine the model parameters were discussed and used to determine AFC model fits to two concrete materials. The AFC model was used in a finite element code to conduct numerical simulations of perforation and penetration experiments in order to validate the new model. The validated model was used in the VPL code to develop a PR equation for the CSPC concrete. Finally, the PR equation was used in a rigid-body trajectory code to create a fast-running penetration model.

The numerical simulations conducted using the AFC model provided predictions of penetration depths, perforation velocities, and crater shapes comparable to those from full finite element simulations. These initial results indicate that the AFC model shows significant promise for being a useful constitutive model for use in simulations involving concrete and geologic materials.

Acknowledgments

The research reported herein was conducted as part of the U.S. Army Corps of Engineers Survivability and Protective Structures Technical Area, Hardened Combined Effects Penetrator Warheads Work Package, Work Unit "HPC Prediction of Weapon Penetration, Blast and Secondary Effects". Permission to publish was granted by Director, Geotechnical and Structures Laboratory.

References

Adley, M.D., Frank, A.O., Danielson, K.T., Akers, S.A. and O'Daniel, J.L. (2007), "Penetration resistance functions for projectile structural response simulations", *Proceedings of Symposium on Plasticity and Impact Mechanics*, Bochum, Germany.

Adley, M.D., Cargile, J.D., Akers, S.A. and Rohani, B. (1996), "Numerical simulation of projectile penetration into concrete", *Proceedings of the 14th U.S. Army Symposium on Solid Mechanics*, Myrtle Beach, SC.

Akers, S.A., Adley, M.D. and Cargile, J.D. (1995), "Comparison of constitutive models for geologic materials used in penetration and ground shock calculations", *Proceedings of the 7th International Symposium on the Interaction of Conventional Munitions with Protective Structures*, Mannheim FRG.

Bažant, Z.P., Caner, F.C., Carol, I., Adley, M.D. and Akers, S.A. (2000), "Microplane model M4 for concrete. I: Formulation with work-conjugate stress", *J. Eng. Mech.*, **126**(9), 944-953.

Bažant, Z.P., Xiang, Y., Adley, M. D., Prat, P.C. and Akers, S.A. (1996), "Microplane model for concrete. I: Stress-strain boundaries and finite strain; II: Data delocalization and verification", *J. Eng. Mech.*, **122**(3), 245-262.

Cargile, J.D. (1999), "Development of a constitutive model for numerical Simulations of projectile penetration into brittle geomaterials", Technical Report SL-99-11, U.S. Army Engineer Research and Development Center, Vicksburg, MS.

Chen, W.F. and Han, D.J. (1988), *Plasticity for Structural Engineers*, Springer-Verlag, NY.

Fossum, A.F. and Brannon, R.M. (2006), "On a viscoplastic model for rocks with mechanism-dependent characteristic times", *Acta Geotechnica*, **1**, 89-106.

Frew, D.J., Cargile, J.D. and Ehrgott, J.Q. (1993), "WES geodynamics and projectile penetration research facilities", *Proceedings of the Symposium on Advances in Numerical Simulation Techniques for Penetration and Perforation of Solids*, ASME Winter Annual Meeting, New Orleans, LA.

Furukawa, T., Sugata, T., Yoshimura, S. and Hoffman, M. (2002), "An automated system for simulation and parameter identification of inelastic constitutive models", *Comput. Method. Appl. M.*, **191**, 2235-2260.

Holmquist, T.J., Johnson, G.R. and Cook, W.H. (1993), "A computational constitutive model for concrete subjected to large strains, high strain rates, and high pressures", *Proceedings of the Fourteenth International Symposium on Ballistics*, Quebec City, Canada.

Johnson, G.R., Stryk, R.A. and Beissel, S.R. (2001) "User instructions for the 2001 version of the EPIC code", Alliant Techsystems Inc., Hopkins, MN.

Marquardt, D. (1963), "An algorithm for least-squares estimation of nonlinear parameters", *SIAM J. Appl. Math.*, **11**, 431-441.

Ožbolt, J., Periškic, G., Reinhardt, H-F. and Eligehausen, R. (2008), "Numerical analysis of spalling of concrete cover at high temperature", *Comput. Concrete*, **5**(4), 279-293.

Ožbolt, J., Kozar, I., Eligehausen, R. and Periškic, G. (2005), "Three-dimensional FE analysis of headed stud anchors exposed to fire", *Comput. Concrete*, **2**(4), 249-266.

Parichatprecha, R. and Nimityongskul, P. (2009), "An integrated approach for optimum design of HPC mix Pproportion using genetic algorithm and artificial neural networks", *Comput. Concrete*, **6**(3), 253-268.